https://doi.org/10.3311/PPch.43057

Periodica Polytechnica Chemical Engineering

Photocatalytic Degradation of Metformin Using ZnO/UV System: Kinetic Study and Transport Modeling in Porous Media

Wassila Hachi[1*], Farida Kaouah[1], Hamza Bouredji[2], Nadia Bendjaballah-Lalaoui[3]

[1] Laboratory of Industrial Process Engineering Sciences, Faculty of Mechanical Engineering and Process Engineering, University of Science and Technology Houari Boumediene, Algiers 16111, Algeria
[2] Laboratory of Advanced Solutions in Process Engineering, Department of Process Engineering, Faculty of Technology, University of Batna 2 Mostefa Ben Boulaïd, Batna 05078, Algeria
[3] Laboratory of Catalytic Materials and Catalysis in Organic Chemistry, University of Science and Technology Houari Boumediene, Algiers 16111, Algeria
* Corresponding author, e-mail: hachi_wassila@yahoo.fr

Received: 11 December 2025, Accepted: 18 May 2026, Published online: 20 July 2026

Abstract

The occurrence of pharmaceutical contaminants in aquatic and terrestrial environments has become a major environmental concern due to their persistence, continuous release, and biological activity at low concentrations. Metformin hydrochloride, a widely prescribed antidiabetic drug, is frequently detected in water and soil systems owing to its high consumption and resistance to biodegradation. This work couples photocatalysis with soil transport modeling to assess removal efficiency and environmental fate.This study investigates the transformation of metformin from aqueous solutions using ZnO-assisted photocatalysis under UV irradiation, combined with an assessment of its transport behavior in porous media. The influence of key operational parameters, including catalyst loading, initial concentration, and pH, was systematically evaluated. Under optimal conditions (pH 9.7, 0.3 g L^{-1} ZnO), a removal efficiency of 77% was achieved within 180 min. Kinetic analysis confirmed pseudo-first-order behavior, demonstrating the effectiveness of photocatalysis compared to adsorption alone. It should be noted that UV–Vis spectrophotometry reflects primary transformation rather than complete degradation due to the possible formation of transformation products such as guanylurea. The transport of metformin was further simulated in light sand and biosolid-amended soil using a nonlinear physical nonequilibrium (PNE) model. Breakthrough curve analysis revealed rapid transport with limited retention in lignt sand, whereas delayed migration and enhanced sorption were observed in biosolid-amended soil, indicating nonlinear sorption behavior. These findings highlight the importance of integrating advanced treatment processes with subsurface transport analysis to provide a more comprehensive environmental risk assessment of pharmaceutical contaminants.

Keywords

metformin, ZnO, advanced oxidation processes, soil transport, breakthrough curves

1 Introduction

The accelerated industrialization and urbanization of recent decades have resulted in widespread and persistent contamination of aquatic and terrestrial environments by a wide range of organic pollutants, including pharmaceuticals, pesticides, dyes, and other anthropogenic compounds [1–3]. Among these emerging contaminants, active pharmaceutical ingredients (APIs) represent a growing environmental concern due to their continuous release, environmental persistence, biological activity at trace concentrations, and potential for bioaccumulation [1, 2]. Unlike conventional pollutants regulated by strict discharge standards, pharmaceuticals are continuously introduced into the environment through multiple pathways, including municipal wastewater effluents, hospital discharges, agricultural runoff, and the land application of biosolids [2, 4]. Once released, these compounds may persist in aquatic systems, accumulate in sediments, or migrate into groundwater through subsurface transport, thereby creating secondary pollution sources [1, 3]. Their incomplete degradability, combined with intrinsic bioactivity, makes APIs

Cite this article as: Hachi, W., Kaouah, F., Bouredji, H., Bendjaballah-Lalaoui, N. "Photocatalytic Degradation of Metformin Using ZnO/UV System: Kinetic Study and Transport Modeling in Porous Media", Periodica Polytechnica Chemical Engineering, 2026. https://doi.org/10.3311/PPch.43057

particularly problematic contaminants requiring integrated assessment across both water and soil systems [1]. Metformin hydrochloride (MET), chemically known as 3-(diaminomethylidene)-1,1-dimethylguanidine hydrochloride, exemplifies this issue. As one of the most widely prescribed antidiabetic drugs for type II diabetes worldwide, metformin is produced and consumed in large quantities. Due to its low metabolic degradation in the human body, approximately 50% of the administered dose is excreted unchanged in urine [5]. Consequently, metformin is frequently detected in wastewater, surface waters, and increasingly in soils receiving treated wastewater or biosolids [5, 6]. Its high polarity, chemical stability, and resistance to biodegradation contribute to its persistence in the environment, making it a suitable model compound for studying both treatment efficiency and environmental fate.

Conventional water treatment processes, such as coagulation, flocculation, and adsorption, are generally ineffective for the removal of pharmaceutical compounds and often result in phase transfer rather than complete elimination [2, 3]. In contrast, advanced oxidation processes (AOPs), based on the generation of highly reactive hydroxyl radicals (•OH), have emerged as effective alternatives due to their strong oxidative potential and non-selective reactivity toward a wide range of organic contaminants [1, 2]. Among these technologies, heterogeneous photocatalysis has attracted considerable attention because of its operational simplicity, cost-effectiveness, and potential for solar-driven applications [3, 7]. Zinc oxide is a particularly promising photocatalyst owing to its favorable physicochemical properties, including a wide band gap ($E_g \approx 3.2$ eV), high exciton binding energy, chemical stability, low cost, and relatively low toxicity [7, 8]. Numerous studies have reported the photocatalytic transformation of metformin using ZnO under UV irradiation, focusing primarily on optimizing operational parameters and evaluating kinetic behavior. However, these studies are generally limited to aqueous phase treatment and do not address the subsequent environmental fate of treated effluents. The critical limitation of current research lies in the assumption that removal from water equates to environmental safety. In reality, residual metformin and its transformation products may enter soil systems through irrigation with treated wastewater or biosolid application. Once in the subsurface, their mobility is governed by soil properties, sorption mechanisms, and hydrodynamic conditions, which ultimately control the risk of groundwater contamination.

While numerous studies have reported the photocatalytic degradation of metformin using ZnO under UV irradiation, these works are generally limited to aqueous phase treatment and focus primarily on process optimization and kinetic analysis. However, they do not address the subsequent environmental fate of treated effluents, particularly their behavior in soil systems. The novelty of the present study lies in coupling photocatalytic degradation kinetics with subsurface transport modeling using a nonlinear physical non-equilibrium (PNE) model. This integrated approach provides a more comprehensive understanding of the environmental fate of metformin by linking its transformation in water to its mobility and persistence in porous media. To date, no study has comprehensively coupled photocatalytic transformation with subsurface transport modeling to evaluate the environmental fate of metformin across multiple environmental compartments. Addressing this gap is essential for developing a more realistic and integrated framework for environmental risk assessment. In this context, the present study proposes a dual approach. First, the photocatalytic transformation of metformin using a ZnO/UV system is systematically investigated, including the comparison between adsorption and photocatalysis, optimization of operational parameters, catalyst characterization, and kinetic modeling based on pseudo-first-order and Langmuir–Hinshelwood (L-H) approaches. Second, the transport behavior of metformin is simulated in two contrasting porous media (light sand and biosolid-amended soil) using a nonlinear PNE model, accounting for mass transfer limitations and nonlinear sorption. By integrating photocatalytic transformation with subsurface transport modeling, this study provides a comprehensive framework for understanding the environmental fate of pharmaceutical contaminants, bridging the gap between water treatment efficiency and long-term environmental behavior.

2 Materials and methods

2.1 Chemical reagents

Commercial zinc oxide (99% purity) supplied by Merck was used as the photocatalyst. According to the manufacturer, the particle size ranged from 0.1 to 4 μm, with a specific surface area (S_{BET}) of approximately 9 $m^2\ g^{-1}$. Metformin hydrochloride (99% purity), obtained from Sigma-Aldrich, was used as the target compound. Its main physicochemical properties are summarized in Table 1, and its chemical structure is presented in Fig. 1. A stock solution of metformin was prepared by dissolving

Table 1 Physicochemical properties of metformin hydrochloride

Types of properties	Paramteres	Values
Physical properties	Physical state	Solid
	Appearance	White powder
	Water solubility (25 °C)	300 g/L
	Melting point	223-226 °C
	Boiling point	267 °C
	λ_{max}	233 nm
Chemical properties	Chemical formula	$C_4H_{11}N_5$
	Molar mass	129.20 g/mol
	pKa	3.10-13.80

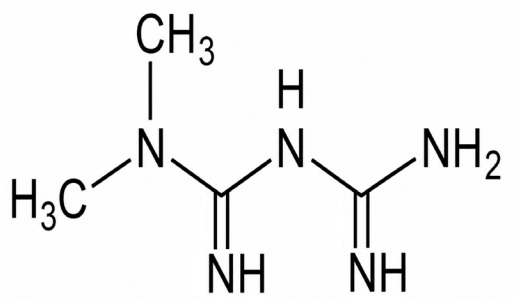

Fig. 1 Chemical structure of metformin

the required amount in distilled water. The solution was stirred in the dark for 3 h to ensure complete dissolution and stabilization before use. Working solutions of the desired concentrations were then obtained by dilution. The pH of the solutions was adjusted using hydrochloric acid and sodium hydroxide. Metformin was selected as a model pollutant due to its frequent detection in various environmental compartments [5], its low biodegradability, and its persistence in aqueous and soil systems.

2.2 Experimental setup

All experiments were carried out under artificial irradiation. Photodegradation tests were conducted in batch mode in a cylindrical, jacketed glass reactor (250 mL capacity) connected to a thermostatically controlled water bath, with the temperature maintained at 25 ± 1 °C. Irradiation was provided by a 24 W UV lamp emitting predominantly at 365 nm, mounted on a fixed support and positioned parallel to the plane of the reactor. The distance between the UV source and the solution was kept constant at 5 cm to ensure uniform irradiation. The entire system was enclosed in a sealed chamber lined with aluminum foil to minimize UV losses and prevent interference from external light. The required amount of semiconductor was added to aqueous MET solutions, and the resulting suspension was magnetically stirred overnight in the dark to ensure homogeneous dispersion of the catalyst and to reach adsorption–desorption equilibrium. This step was performed to evaluate the adsorption capacity of MET onto the semiconductor prior to irradiation. After irradiation, samples were withdrawn from the reactor at regular time intervals, centrifuged at 3000 rpm, and analyzed using a UV–visible spectrophotometer. A schematic representation of the experimental setup is provided in Fig. 2.

2.3 Characterization techniques

The crystalline structure of ZnO was determined by X-ray diffraction (XRD) using a Shimadzu D6000 (Japan) diffractometer with Cu-Kα radiation (λ = 1.54 Å) at 40 kV and 3 mA, scanned at 0.2° min^{-1}. Particle morphology was examined by scanning electron microscopy (SEM; Hitachi S-4800, Japan), and particle size distribution was measured using a laser particle size analyzer (Mastersizer 2000, Malvern Instruments, UK). The optical band gap was evaluated by diffuse reflectance spectroscopy (DRS) with a Specord 200 Plus spectrophotometer (Analytik Jena, Germany) over 190–1100 nm. The isoelectric point of the photocatalyst was determined by zeta potential analysis (Zetasizer Nano-ZS, Malvern Instruments, UK) in the pH range 5–11, following the method described by Kosmulski [9].

2.4 Experimental procedures

A fixed amount of catalyst was dispersed in 100 mL of MET solution at the initial concentration (C_0) under moderate stirring (300 rpm) to prevent vortex formation. During UV irradiation, 3 mL samples were withdrawn every 30 min from the batch reactor, centrifuged, and filtered to remove ZnO particles, then analyzed

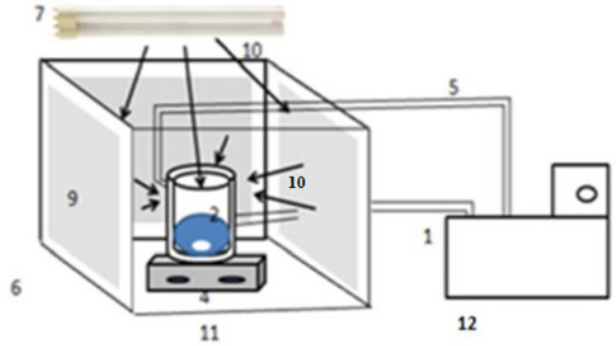

Fig. 2 Schematic diagram of the photocatalytic experimental setup. 1: Water inlet, 2: jacketed reactor, 3: bar magnet, 4: magnetic agitator, 5: out of the water, 6: transparent cover, 7: UV lamp, 8: sampling point, 9: aluminium foil, 10: light reflection, 11: box, 12: thermostatic bath.

by UV–visible spectrophotometry (Specord 200 Plus, λ_{max} = 233 nm). To quantify the contributions of adsorption and photolysis, control experiments were performed in the dark and under UV light in the absence of the catalyst. The degree of mineralization was determined using a total organic carbon (TOC) analyzer (CSH E200, Shimadzu, Japan). The percentage of MET degradation was calculated using Eqs. (1) and (2) [10]:

$$D(\%) = \frac{C_0 - C_t}{C_0} \times 100 \quad (1)$$

$$M(\%) = \frac{T_0 - T_t}{T_0} \times 100\% \quad (2)$$

where D is degradation and M is mineralization efficiency. C_t is the concentration of MET at time t, T_0 is the initial TOC concentration and T_t is the TOC concentration after photocatalysis at time t.

3 Results and discussion

3.1 Characterization of the photocatalyst

The band gap energy (E_g) of ZnO, a key parameter governing its photocatalytic activity, was determined from diffuse reflectance spectroscopy measurements. The band gap was estimated by extrapolating the linear region of the Tauc plot of $(\alpha h\nu)^2$ as a function of the photon energy ($h\nu$), according to Eq. (3).

$$(\alpha h\nu)^n = \text{const}(h\nu - E_g) \quad (3)$$

where α is the optical absorption coefficient and $n = 2$.

The band gap energy of ZnO was estimated to be 3.20 ± 0.02 eV (Fig. 3).

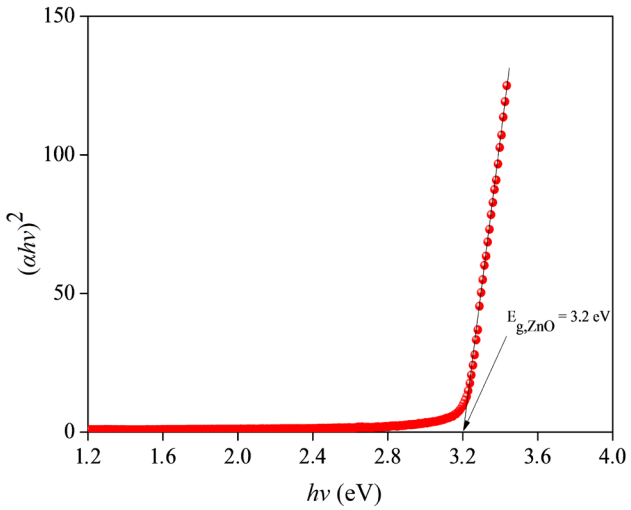

Fig. 3 Direct band gap transition of ZnO

The X-ray diffraction pattern of ZnO, recorded over a 2θ range of 20–100°, is presented in Fig. 4. All diffraction peaks can be indexed to the hexagonal wurtzite structure of ZnO, in good agreement with the standard ICDD PDF card No. 36-1451 [11], confirming the high crystallinity of the material.

Zeta potential measurements were performed to evaluate the surface charge and colloidal stability of ZnO particles. A high absolute value of zeta potential indicates strong electrostatic repulsion between particles, thereby reducing aggregation and improving dispersion stability. The variation of zeta potential as a function of pH is shown in Fig. 5.

The point of zero charge (pH_{pzc}) of ZnO was determined to be approximately 9.2, providing important insight into the interactions between the ZnO surface and metformin molecules. At pH values below 9.2, the ZnO surface is positively charged (Eq. 4), whereas at pH values above 9.2, it becomes negatively charged (Eq. 5). At the optimal pH (≈ 9.7), ZnO carries a negative surface charge, while metformin is predominantly present in its monocationic form, leading to electrostatic attraction that enhances adsorption and photocatalytic transformation.

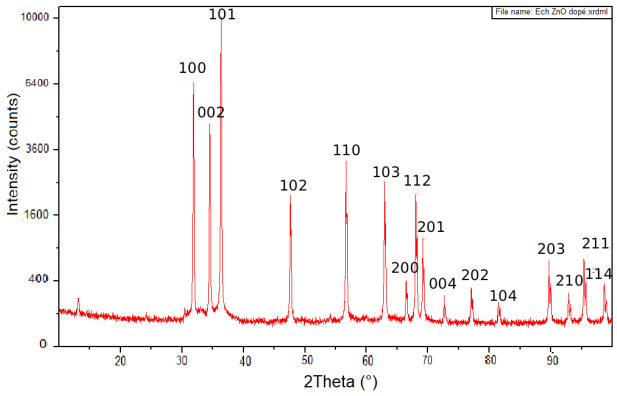

Fig. 4 X-ray diffraction pattern of ZnO

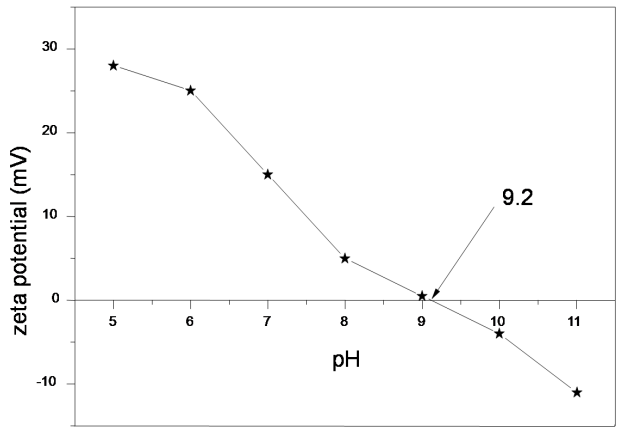

Fig. 5 Zeta potential of ZnO as a function of solution pH and the point of zero charge (pH_{pzc})

$$Zn-OH+H^{+} \rightarrow Zn-OH_2^{+} \quad (4)$$

$$Zn-OH+OH^{-} \rightarrow Zn-O^{-} \quad (5)$$

The SEM image (Fig. 6) reveals that the ZnO sample consists of agglomerated fine particles forming porous clusters, which may enhance the available surface area for photocatalytic reactions. The particle size ranges from approximately 0.35 to 2 µm, with more than 90% of the particles being smaller than 0.55 µm.

3.2 Preliminary comparison of removal

The performance of heterogeneous photocatalysis using ZnO was evaluated by comparing three different processes for the removal of MET: adsorption, photolysis, and photocatalysis. In the adsorption experiments, the MET solution was brought into contact with ZnO in the absence of irradiation, allowing the catalyst to act solely as an adsorbent. In the photolysis experiments, the MET solution was exposed to UV irradiation without the presence of ZnO. In contrast, photocatalytic experiments were carried out under simultaneous UV irradiation and ZnO addition, enabling both adsorption and photocatalytic transformation. All experiments were performed at an initial MET concentration of 20 mg·L^{-1}. The ZnO dosage ranged from 0.05 to 0.5 g L^{-1}, and the natural pH of the solution was approximately 6.4. Fig. 7 illustrates that during adsorption, which is a purely physical process, MET was only slightly removed, with a removal efficiency of less than 9%. The presence of UV light alone resulted in a low removal

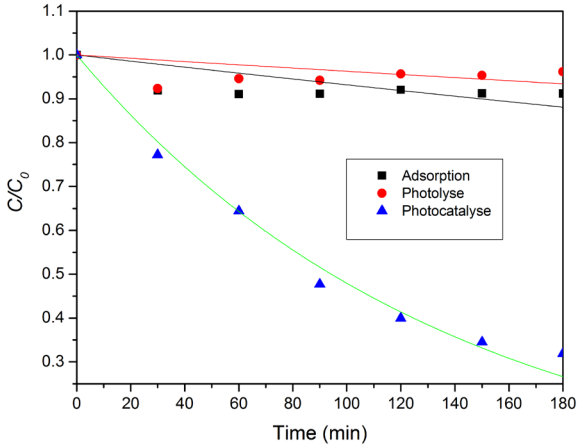

Fig. 7 Temporal evolution of MET concentration during different processes

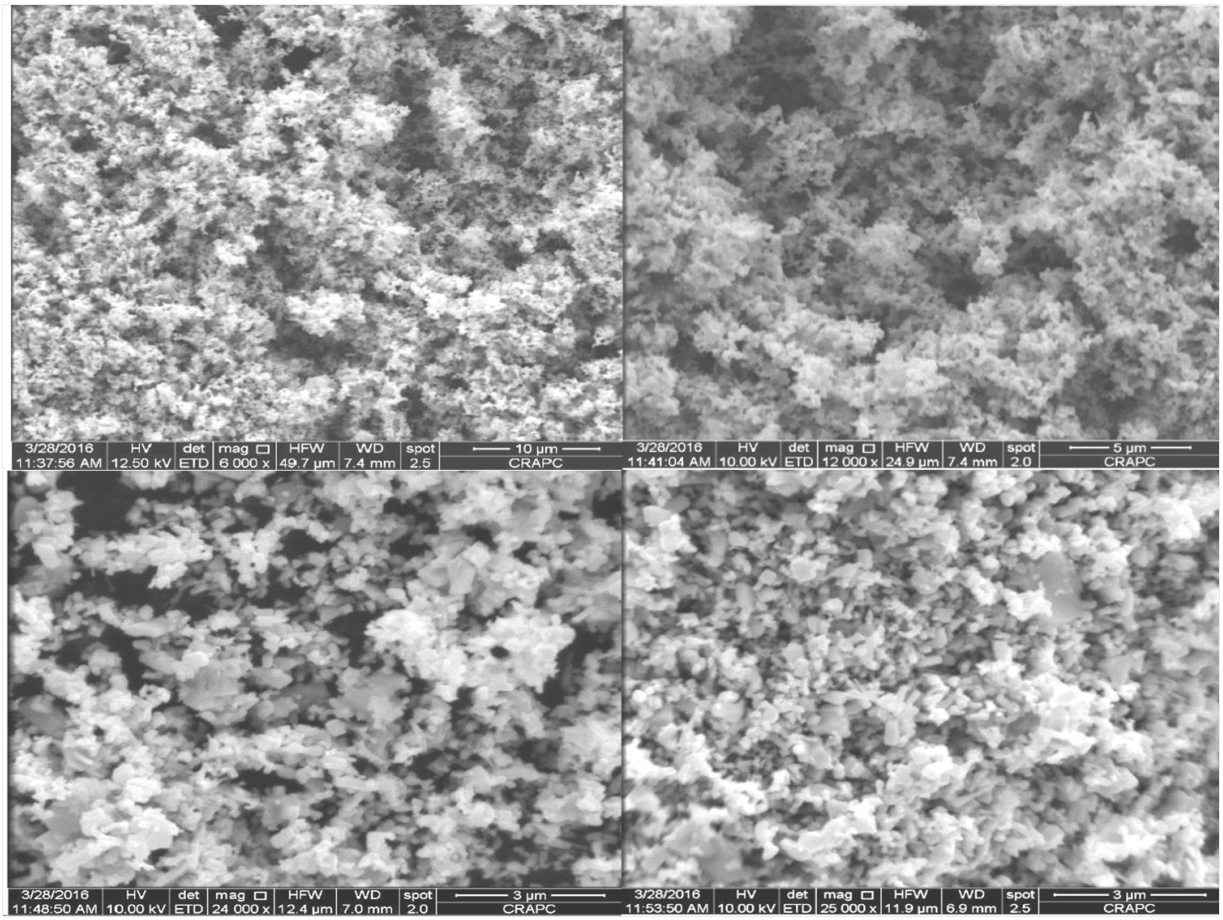

Fig. 6 SEM image of ZnO

rate, not exceeding 8%. These observations are consistent with the findings of Tao et al. [12], who reported that MET removal after 2 h of photolysis was not significant.

In contrast, photocatalysis in the presence of ZnO under a 24 W UV lamp significantly enhanced MET transformation, achieving 70% removal after 180 min of irradiation. Similarly, De la Cruz et al. [13] reported that the photocatalytic transformation of a pharmaceutical compound under artificial irradiation reached 71% removal after 240 min.

3.3 Kinetic analysis

3.3.1 Evaluation of the reaction order

The photocatalytic transformation of MET was investigated at initial concentrations ranging from 10 to 40 mg L^{-1}, using a ZnO dosage of 0.3 g L^{-1} at natural pH conditions. The reaction kinetics were analyzed using both linear and nonlinear approaches based on the pseudo-first-order model:

$$\frac{dC}{dt} = -k_{app} \times C \,, \tag{6}$$

$$C = C_0 \exp\left(-k_{app} \times t\right), \tag{7}$$

where k_{app} is the apparent pseudo-first-order rate constant. The nonlinear fitting results (Fig. 8) show good agreement with the experimental data, confirming the applicability of the pseudo-first-order model [14]. This behavior is consistent with the Langmuir–Hinshelwood (L–H) mechanism, where at low concentrations the reaction rate is proportional to the pollutant concentration. Slight deviations at higher concentrations are attributed to light attenuation and partial saturation of active sites.

3.3.2 Photocatalytic activity kinetics

Effect of ZnO dosage

The kinetics of metformin transformation under UV irradiation were investigated by monitoring the temporal evolution of its concentration in solution. To better understand and optimize the photocatalytic process, key operational parameters, including catalyst loading, solution pH, and initial MET concentration, were systematically varied. All experiments were conducted under the conditions described above. Catalyst dosage is a critical parameter in heterogeneous photocatalysis systems operating in suspension. An optimal amount ensures maximum efficiency at minimal cost and depends on both the nature of the pollutant and the reactor configuration [15]. Previous studies have

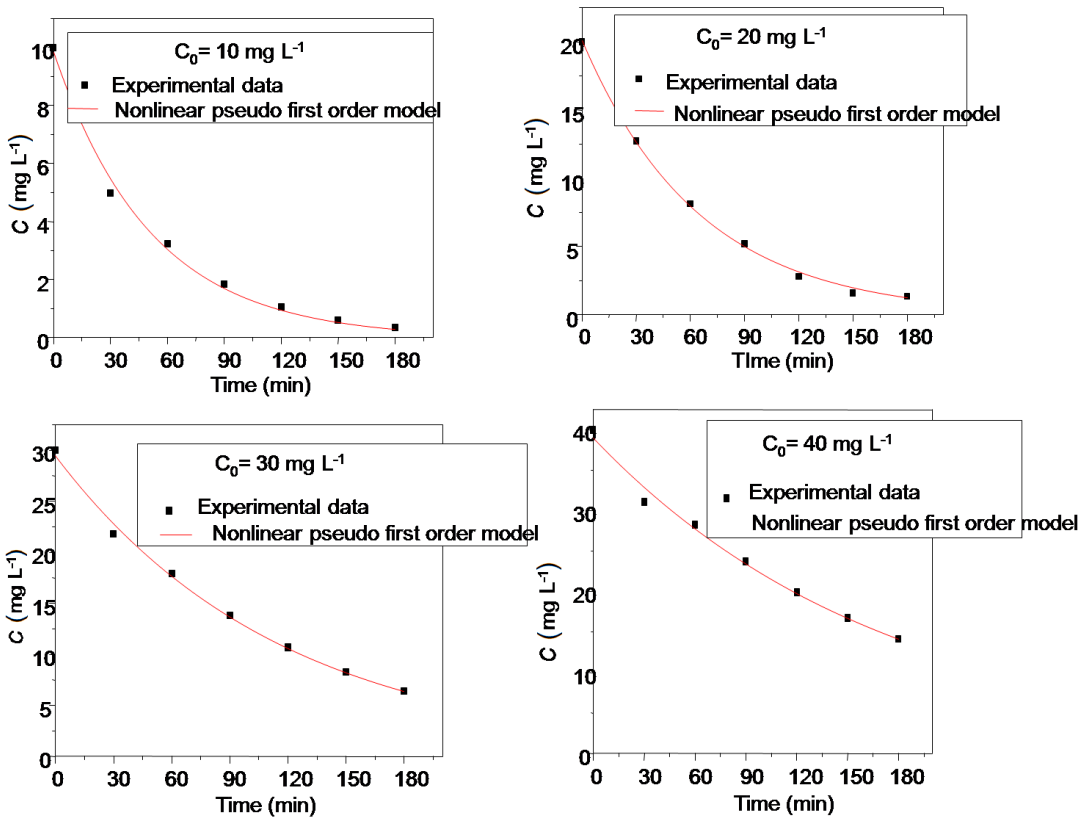

Fig. 8 Nonlinear plots of the pseudo-first-order kinetic model at different initial MET concentrations for photocatalytic degradation over ZnO

demonstrated the existence of an optimal catalyst loading for effective pollutant transformation [16, 17]. The effect of ZnO dosage on the transformation rate of MET was investigated over the range of 0–0.5 g L^{-1} under UV irradiation, using an initial MET concentration of 20 mg L^{-1} at natural pH. The corresponding results are presented in Fig. 9.

In the absence of ZnO, the MET concentration remains nearly constant, with a transformation efficiency not exceeding 8% after 180 min of irradiation, confirming that direct photolysis plays a negligible role. Therefore, the observed removal can be mainly attributed to the photocatalytic process. The results clearly show that ZnO dosage has a significant effect on MET transformation. The transformation efficiency increases with increasing catalyst concentration, reaching a maximum of approximately 69% at 0.2 g L^{-1} (Fig. 10).

This behavior is attributed to the increase in the number of available active sites and enhanced photon absorption. However, beyond this optimal dosage, a decrease in transformation efficiency and the corresponding apparent rate constants (Table 2) is observed. This decline can be attributed to light scattering, reduced light penetration, and particle aggregation at higher catalyst concentrations, which limit the effective photocatalytic activity. At elevated ZnO loadings, a screening effect occurs due to increased turbidity and light scattering within the suspension. This phenomenon reduces light penetration and limits the generation of reactive species, particularly hydroxyl radicals (•OH), which are responsible for the oxidation of metformin [18, 19]. Since photocatalysis is a surface-driven process, the kinetic parameters strongly depend on the effective surface area exposed to irradiation. As shown in Table 2, the half-life ($t_{1/2}$) decreases as the ZnO dosage increases from 0 to 0.2 g L^{-1}, while the corresponding apparent rate constants increase over the same range.

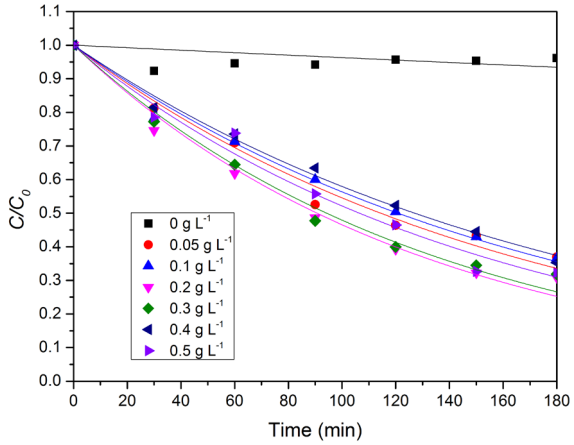

Fig. 9 Photocatalytic removal of MET at different ZnO dosages

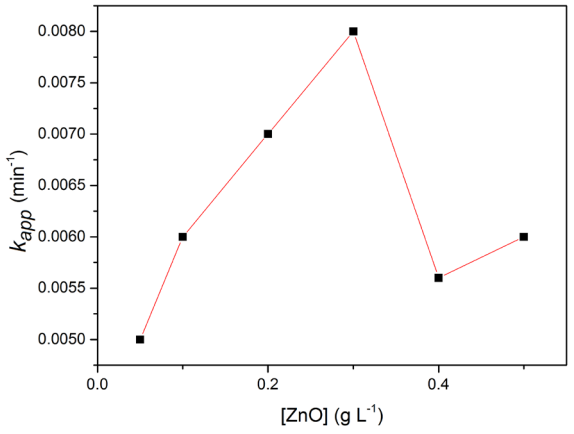

Fig. 10 Variation of the apparent rate constant as a function of ZnO dosage

Several studies have reported that the influence of catalyst dosage on transformation kinetics can be empirically described by a power-law relationship between the apparent rate constant and catalyst concentration [20, 21]:

$$\ln k_{app} = \ln k_1 + n_{app} \ln[\mathrm{ZnO}], \tag{8}$$

where [ZnO] represents the concentration of ZnO in the reaction medium, k_1 is the kinetic constant. n_{app} is defined as the apparent reaction order with respect to ZnO concentration. Applying Eq. (8) to the experimental results yields a linear relationship (Fig. 11), from which an apparent reaction order of 0.26 with respect to ZnO concentration was determined under artificial irradiation. The apparent rate constants can thus be expressed empirically as:

$$k_{app} = 2.03\times10^{-3}[\mathrm{ZnO}]^{0.26} \tag{9}$$

The obtained fractional reaction order ($n < 1$) indicates that the dependence of the reaction rate on catalyst concentration is non-linear. This behavior does not reflect a

Table 2 Kinetic parameters, initial reaction rates, and half-life for metformin transformation at different ZnO dosages

[ZnO] (gL^{-1})	R (%)	k_{app} (min^{-1})	r_0 (mgL^{-1}·min^{-1})	$t_{1/2}$ (min)	R^2
0	8	3.74×10^{-4}	0.051	1.85×10^{3}	/
0.05	63	0.00588	0.125	1.18×10^{2}	0.96988
0.1	63	0.00566	0.145	1.22×10^{2}	0.99199
0.2	69	0.00728	0.17	9.52×10^{1}	0.96997
0.3	68	0.00704	0.152	9.85×10^{1}	0.96885
0.4	64	0.00552	0.124	1.26×10^{2}	0.99145
0.5	67	0.0066	0.143	1.05×10^{2}	0.9728

Note: R corresponds to the degradation percentage, r_0 represents the initial rate, and R^2 is the coefficient of determination.

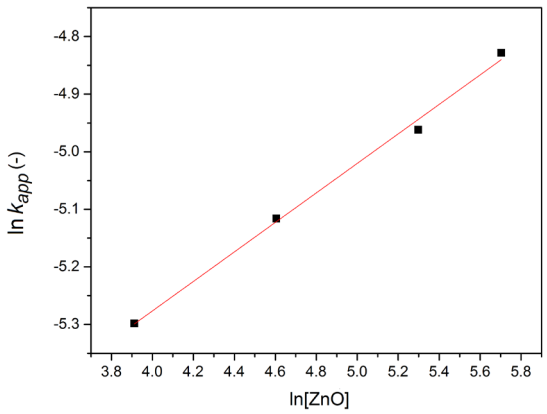

Fig. 11 Variation of lnk_{app} as a function of ln[ZnO]. [ZnO] is expressed in g L^{-1}.

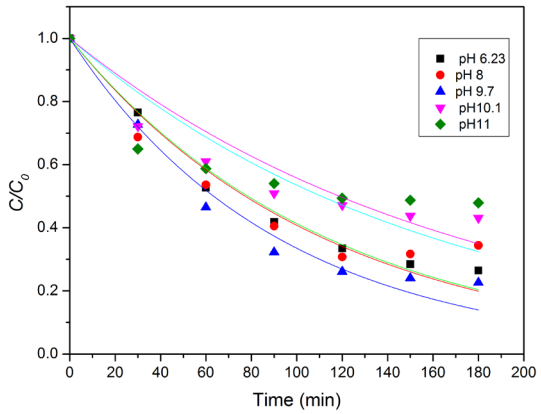

Fig. 12 Photocatalytic degradation of MET at different solution pH values

true mechanistic reaction order but rather results from the combined effects of light attenuation, catalyst aggregation, and mass transfer limitations at higher ZnO concentrations. Similar observations have been reported by Galindo et al. [18] for the photocatalytic degradation of organic compounds. At low catalyst loadings, the reaction rate increases with ZnO concentration due to the higher availability of active sites and improved photon absorption. However, at higher loadings, deviations from linearity occur as a result of light screening effects and partial saturation of the catalyst surface, which limit the effective utilization of the photocatalyst. Therefore, Eq. (8) is valid only within a limited range of ZnO concentrations, where these limiting effects remain negligible.

Effect of solution pH

The pH of the solution is a crucial parameter in photocatalytic processes, as it governs several key factors, including the surface charge of the catalyst, the ionization state of the pollutant, and the generation of reactive oxidative species such as hydroxyl radicals. ZnO is an amphoteric semiconductor characterized by a pH_{pzc} in the range of 9.0–9.2. Consequently, its surface is positively charged at pH < pH_{pzc} and negatively charged at pH > pH_{pzc}. Furthermore, the ionic nature of the pollutant and its interaction with the catalyst surface are strongly influenced by pH variations [22]. The influence of the initial solution pH on the photocatalytic removal of MET was investigated under artificial UV irradiation over a pH range of 6.3–11, with an initial MET concentration of 20 mg L^{-1} and a catalyst loading of 0.2–0.3 g L^{-1}. The pH of the suspension was adjusted prior to irradiation.

As illustrated in Fig. 12, the removal efficiency increases with increasing pH, reaching a maximum value of 77.34% at pH 9.7, followed by a decrease at higher pH values. This behavior can be attributed to the combined effects of catalyst surface charge, MET speciation, and hydroxyl radical formation. Metformin is a polyprotic compound (pKa ≈ 11.5) and exists predominantly in a monocationic form within the investigated pH range (6–11). At pH values close to 9.7, which are slightly above the pH_{pzc} of ZnO, the catalyst surface becomes negatively charged, while MET remains positively charged. This results in strong electrostatic attraction between MET molecules and the ZnO surface, thereby enhancing adsorption and facilitating photocatalytic degradation [23]. In parallel, increasing pH leads to an increase in hydroxide ion concentration, which promotes the formation of •OH through their reaction with photogenerated holes (h^+). These radicals are highly oxidative and play a major role in the degradation mechanism of organic pollutants [24]. This behavior is also consistent with the pH-dependent variation of hydroxyl radical generation efficiency, which directly influences the overall photocatalytic reaction rate.

The apparent rate constant (k_{app}), presented in Fig. 13 and Table 3, follows the same trend, increasing with pH up to 9.7 and decreasing thereafter. At pH values above 10,

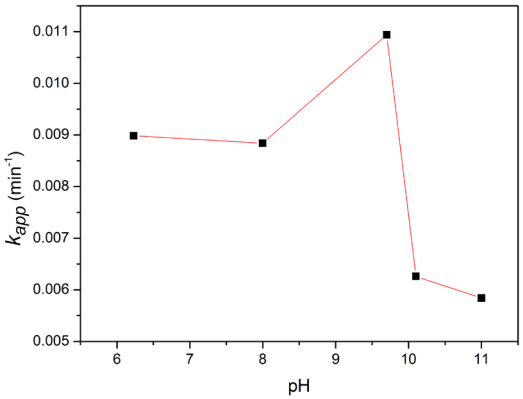

Fig. 13 Variation of the k_{app} as a function of solution pH

Table 3 Kinetic parameters, initial reaction rates, and half-life times for MET removal at different pH values

pH	R (%)	k_{app} (min^{-1})	r_0 ($mg L^{-1} \cdot min^{-1}$)	$t_{1/2}$ (min)	R^2
6.23	73	0.00898	0.0079	77.19	0.98033
8	65	0.00884	0.0078	78.41	0.90978
9.7	77	0.01094	0.0089	63.35	0.97067
10.1	57	0.00626	0.0065	110.72	0.86403
11	64	0.00584	0.0068	118.69	0.63865

the observed decrease in removal efficiency may be attributed to several factors. First, excess OH^- ions may compete with MET molecules for adsorption sites on the catalyst surface. Second, high OH^- concentrations may promote the recombination of photogenerated electron–hole pairs, thereby reducing the availability of reactive species. Third, changes in MET speciation at higher pH may reduce its affinity for the catalyst surface [25].

Similar trends have been reported for ZnO-based photocatalytic systems, confirming that the effect of pH is governed by a complex interplay between electrostatic interactions, radical generation, and dissociation equilibria of the involved species [26]. Overall, the influence of pH on MET photodegradation is governed by multiple interdependent factors, including catalyst surface chemistry, pollutant speciation, and reactive species dynamics, making its interpretation inherently complex.

3.3.3 Mineralization

In photocatalytic degradation processes, the formation and accumulation of intermediate products are of significant concern due to their potential risks to human health and the environment [27]. Therefore, evaluating the extent of mineralization through TOC removal is essential to assess the overall efficiency of the process.

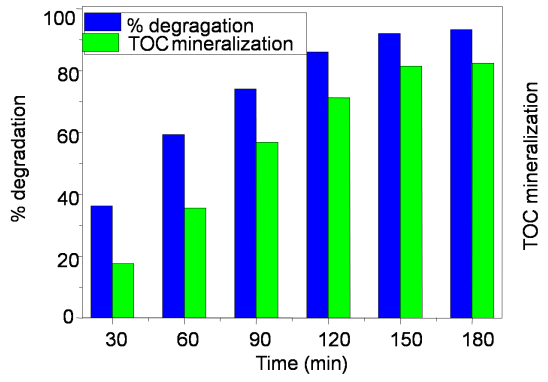

Fig. 14 Comparison of metformin degradation and TOC removal (%) as a function of irradiation time

Fig. 14 presents a comparison between the degradation efficiency of metformin and TOC removal as a function of irradiation time, under the following operating conditions: initial MET concentration of 20 mg L^{-1}, ZnO dosage of 0.3 g L^{-1}, and pH 10. As shown in Fig. 14, after 30 min of irradiation, the degradation of MET reached 36.3%, whereas TOC removal did not exceed 17.67%. This discrepancy indicates that, although MET is transformed, complete mineralization is not achieved at this stage. The relatively slow decrease in TOC during the initial period can be attributed to the formation of intermediate products with lower molecular weight, which still contribute to the overall organic carbon content of the solution. With increasing irradiation time, both MET transformation and TOC removal progressively improve. After 180 min, MET removal and TOC reduction reached 93.28% and 82.37%, respectively. The higher removal efficiency compared to TOC reduction confirms that the photocatalytic process initially favors the transformation of the parent compound, followed by the gradual oxidation of intermediate species toward final mineralization products such as CO_2 and H_2O.

These results highlight that UV–ZnO photocatalysis is effective for the transformation of MET, while complete mineralization requires longer irradiation times due to the sequential oxidation of intermediate by-products.

3.4 Modeling of degradation kinetics

Several studies have shown that heterogeneous photocatalysis can be described by the L–H model [14, 19, 23, 28]. According to this model, organic molecules are first adsorbed onto the catalyst surface, and the initial degradation rate (r_0) is expressed as:

$$r_0 = -\frac{dC}{dt} = \frac{k_r \times K_{L-H} \times C_0}{1 + K_{L-H} \times C_0}, \tag{10}$$

where r_0 is the initial degradation rate, K_{L-H} is the MET adsorption constant on the catalyst, k_r is the reaction rate constant and C_0 is the initial concentration of the organic compound.

The fitting of the experimental MET degradation data using the L–H model (Fig. 15) allowed the determination of the kinetic parameters, as summarized in Table 4.

As shown in Fig. 15, the initial transformation rate increases with increasing initial MET concentration, indicating enhanced interaction between the pollutant and the catalyst surface [29]. Table 4 shows that the L–H model provides a good fit to the experimental data, with coefficient of determination (R^2) higher than 0.975.

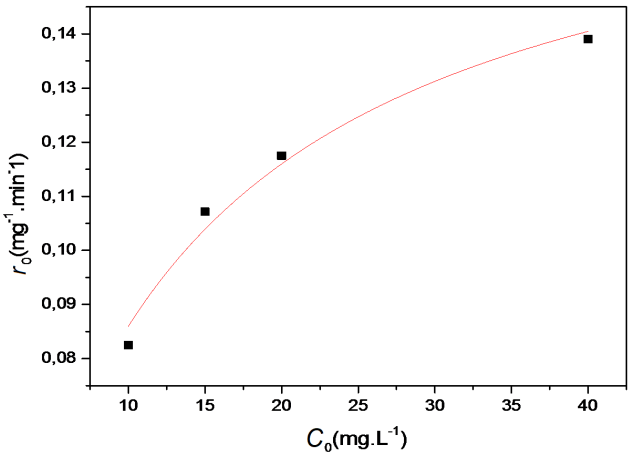

Fig. 15 Application of the Langmuir–Hinshelwood model

Table 4 Kinetic parameters for MET degradation at different initial concentrations

Constants	Values
K_{L-H} (Lmg^{-1})	0.178
K_r (mgL^{-1}·min^{-1})	0.093
R^2	0.975

3.5 Modeling of metformin transport through soil

The transport of MET through soil was investigated using a nonlinear physical non-equilibrium (PNE) model [30, 31]. The breakthrough curves were generated using adsorption and transport parameters obtained from Bouredji et al. [32] for solute transport in saturated porous media, rather than from experimental column studies. No local measurements of soil parameters were conducted; all model inputs were derived from the literature or adapted from previously published values based on adsorption isotherm and kinetic models [33–35]. This modeling approach provides a preliminary assessment of MET mobility and breakthrough behavior under continuous flow conditions, offering insights into adsorption–desorption dynamics and potential environmental risks [34, 35]. It should be noted that the results are predictive in nature, as no experimental validation has been performed. Therefore, the simulated breakthrough curves are theoretical and are intended to illustrate general trends and possible scenarios rather than to provide quantitatively validated outcomes. Future work involving controlled column experiments is required to confirm and refine the model predictions.

3.5.1 Problem formulation

The transport of metformin in a porous medium (soil) with mobile and immobile regions of soil water is governed by the following equations (Leij and Bradford, 2009) [36]:

$$\Theta_m \frac{\partial C_m}{\partial t} + \Theta_m \frac{\partial C_m}{\partial t} + \rho \frac{\partial S_m}{\partial t} + \rho \frac{\partial S_m}{\partial t} = -u_m \times \Theta_m \frac{\partial C_m}{\partial X} + D_m \times \Theta_m \frac{\partial^2 C_m}{\partial X^2}, \quad (11)$$

$$\Theta_{im} \frac{\partial C_{im}}{\partial t} + \rho \frac{\partial S_{im}}{\partial t} = \alpha \times \left(C_m - C_{im}\right), \quad (12)$$

where u_m is the pore-water velocity in the mobile water [LT^{-1}] (where L and T denotes length and time unit, respectively). C_m, C_{im} are the solute concentrations in the mobile and immobile water, respectively [ML^{-3}]. [ML^{-3}] represents mass per unit volume, where M corresponds to mass unit. [MM^{-1}] represents mass of solute per mass of dry soil. Thus, S_m and S_{im} correspond to the concentration of solute adsorbed on the solid phase in the mobile and immobile regions, respectively, expressed as mg of solute per g of dry soil. ρ is the dry soil bulk density [ML^{-3}]. D_m is the hydrodynamic dispersion coefficient in the mobile water phase, representing the spreading of solute caused by velocity variations and molecular diffusion in porous media. Its unit [L^{2}T^{-1}] corresponds to length squared per unit time. X represents the spatial coordinate (distance) along the flow path in the porous medium (m). The variable t represents time in the system. The unit [T] denotes the time dimension, α is the mass transfer coefficient between mobile and immobile regions [1/T]. [L^{3}L^{-3}] corresponds to a volume fraction, representing the ratio of water volume to total porous medium volume. Therefore, Θ_m and Θ_{im} are dimensionless quantities (–).

Equilibrium controlled sorption isotherms are considered in this paper. The Freundlich isotherm model is used:

$$S_m = K_{Fm} \times C_m^n \quad S_{im} = K_{Fim} \times C_{im}^n, \quad (13)$$

where S_m represents the solid-phase concentration of solute adsorbed onto the soil particles in the mobile region, expressed as mass of solute per mass of dry soil. K_{Fm} and K_{Fim} have units (L^3/M)$^{(n,m)}$, where (n,m) denotes an exponent depending on the Freundlich parameter nnn for each region.

Table 5 presents the values of the physical and adsorption parameters of metformin in two types of sandy soils: a light soil (sand + organic matter) and an enriched soil (biosolid). All units are expressed in the International System (SI).

Using the numerical solution of the nonlinear physical non-equilibrium model proposed by Bouredji et al. [37], the transport of metformin through porous media was simulated. The selection of metformin as a target compound is supported by its documented mobility and sorption behavior in soils [38].

Table 5 Soil physicochemical and metformin adsorption parameters for light sand and biosolid- enriched soil

Type of soil	Θ_m (m^3m^{-3})	Θ_{im} (m^3m^{-3})	α (s^{-1}) 10^{-4}	dp (m) 10^{-4}	$K_{Fm} = K_{Fim}$ [(molkg^{-1}) (m^3mol^{-1})$^{1/n}$] 10^{-3}	n
Light sand (sand + organic matter)	0.42	0.10	10	2.5	2.6	0.8
Enriched soil (biosolid)	0.44	0.18	3.0	1.8	10.5	0.6

Note: *dp* represents the particle diameter.

3.5.2 Interpretation of breakthrough curves

Fig. 16 presents the simulated breakthrough curves (BTCs) for metformin transport in light sand and biosolid-enriched soil using the nonlinear physical non-equilibrium (PNE) model. As shown in Fig. 16, the BTCs exhibit distinct transport behaviors depending on the porous medium, reflecting differences in sorption capacity and mass transfer characteristics.

Light sand

The breakthrough curve exhibits a relatively sharp rise followed by a rapid decline, indicating limited retention and moderate adsorption of metformin. This behavior is consistent with a lower Freundlich constant and an exponent closer to unity, suggesting a more linear and less favorable sorption process. In addition, the relatively high mass transfer coefficient indicates faster exchange between mobile and immobile water regions, resulting in reduced tailing.

Biosolid-enriched soil

In contrast, the BTC obtained for biosolid-enriched soil is more asymmetric and shows pronounced tailing, along with a delayed and lower peak concentration. This behavior reflects stronger nonlinear sorption, a higher retention capacity (higher K_F), and slower diffusion into the immobile water fraction (Θ_{im}).

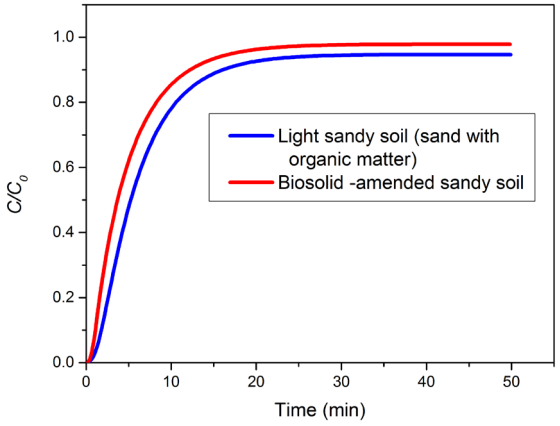

Fig. 16 Simulated breakthrough curves of metformin transport in light sand and biosolid-enriched soil using the nonlinear physical non-equilibrium (PNE) model

The lower mass transfer coefficient further contributes to the extended tailing and delayed release of metformin. These results indicate that biosolid-enriched soil acts as an effective barrier to metformin transport, significantly retarding its migration and reducing the peak concentration reaching groundwater. This effect is primarily attributed to enhanced adsorption capacity and the more complex pore structure of the medium. It should be noted that the BTCs were obtained from numerical simulations and were not validated by experimental column studies. Therefore, the results should be interpreted as a theoretical assessment of metformin transport behavior.

3.5.3 Effect of initial concentration

Figs. 17 and 18 illustrate the influence of the initial metformin concentration (5, 10, 15, and 20 mg L^{-1}) on the

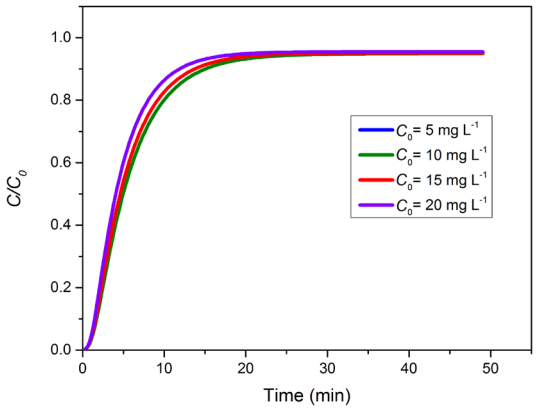

Fig. 17 Simulated breakthrough curves illustrating the effect of initial concentration on metformin transport through light sand

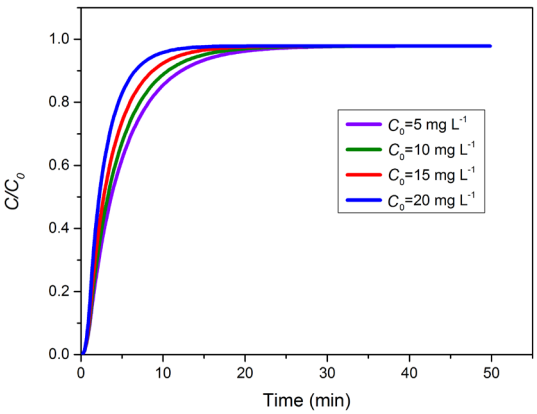

Fig. 18 Simulated breakthrough curves illustrating the effect of initial metformin concentration on transport in biosolid-enriched soil

breakthrough curves in light sand and biosolid-enriched soil, respectively. As shown in Fig. 17, increasing the initial concentration leads to a slight delay in the BTC peak and a more pronounced spreading of the curve. This behavior reflects the nonlinear nature of the Freundlich isotherm ($n = 0.8 < 1$).

At higher concentrations, the available sorption sites become progressively saturated, resulting in a relatively lower fraction of metformin being adsorbed and, consequently, faster relative transport through the porous medium. The increase in the mean breakthrough time (μ_1) with increasing concentration further supports this interpretation. These results confirm the concentration-dependent transport behavior of metformin under nonlinear sorption conditions (Table 6).

It should be noted that transformation products such as guanylurea may exhibit stronger sorption, leading to lower mobility than metformin; however, this study is limited to the parent compound (metformin), and thus the transport behavior of treated effluents may differ.

As shown in Fig. 18, the effect of the initial concentration is more pronounced in biosolid-enriched soil. The breakthrough curves exhibit a significant delay in arrival time and increased spreading as the concentration increases. This behavior reflects strong nonlinear sorption, characterized by a Freundlich exponent ($n = 0.6 < 1$). At low concentrations, the soil exhibits a high affinity for metformin, resulting in substantial retardation. As the concentration increases, this affinity decreases relative to the dissolved amount, leading to a delayed but more concentrated breakthrough. The decrease in relative variance (σ_{r^2}) with increasing concentration suggests a shift toward more equilibrium-like transport conditions at higher solute loadings (Table 7).

The transport of metformin is strongly dependent on the input concentration, with nonlinear sorption leading to earlier relative breakthrough at higher concentrations in both soils. This behavior has important implications for predicting the impact of pulse inputs or accidental releases into subsurface environments.

Table 6 Transport parameters derived from breakthrough curves for metformin in light sand at different initial concentrations

C_0 (mgL^{-1})	μ_1 (min)	σ_{r^2}*	Pe**
5	6.74	2.28	0.008
10	7.51	1.98	0.008
15	8.02	1.83	0.008
20	8.41	1.72	0.008

* The relative variance (σ_{r^2}) is a dimensionless parameter that quantifies the dispersion of data relative to the model prediction, reflecting the goodness of fit between experimental and calculated values.
** Pe represents the Péclet number, which describes the ratio of advective to diffusive transport.

Table 7 Transport parameters derived from breakthrough curves for metformin in biosolid-enriched soil at different initial concentrations

C_0 (mgL^{-1})	μ_1 (min)	σ_{r^2}	Pe
5	3.71	3.84	0.006
10	4.52	2.78	0.006
15	5.20	2.26	0.006
20	5.82	1.94	0.006

4 Conclusion

This study demonstrated the effectiveness of ZnO/UV photocatalysis for the transformation of the pharmaceutical compound metformin and provided important insights into its transport behavior in soil environments. The photocatalytic process was significantly more efficient than adsorption alone, achieving a transformation efficiency of 77% under optimal conditions (pH 9.7 and a ZnO dosage of 0.3 g L^{-1}). The reaction kinetics followed an apparent pseudo-first-order model and were well described by the Langmuir–Hinshelwood mechanism, confirming the surface-controlled nature of the process. A key contribution of this work lies in coupling photocatalytic transformation with subsurface transport modeling, allowing a more comprehensive evaluation of metformin environmental fate. Transport modeling using a nonlinea physical non-equilibrium model revealed that soil composition is a key factor controlling metformin mobility. Light sand exhibited limited retention and rapid breakthrough, whereas biosolid-enriched soil significantly retarded transport, resulting in a delayed and lower peak concentration due to its higher adsorption capacity and greater immobile water content (Θ_{im}). The nonlinear Freundlich isotherm successfully described the concentration-dependent sorption behavior, with higher initial concentrations leading to earlier relative breakthrough, particularly in biosolid-enriched soil. Overall, these results highlight that removal from the aqueous phase does not necessarily imply reduced environmental risk, as transformation products and residual compounds may still migrate in subsurface environments. The integration of advanced oxidation processes with transport modeling, as demonstrated in this study, provides a robust framework for assessing the environmental fate and potential risks of pharmaceutical contaminants.

Acknowledgement

The project presented in this article is supported by the General Directorate for Scientific Research and Technological Development, Ministry of Higher Education and Scientific Research, Algeria.

References

[1] Aziz, K. H., Mustafa, F., Karim, M. A. H., Hama, S. "Pharmaceutical pollution in the aquatic environment: advanced oxidation processes as efficient treatment approaches: a review", Materials Advances, 6(11), pp. 3433–3454, 2025. https://doi.org/10.1039/d4ma01122h

[2] Okeke, E. S., Ezeorba, T. P. C., Okoye, C. O., Chane, Y., Mao, G., Freng, W., Wu, X. "Environmental and health impact of unrecovered API from pharmaceutical manufacturing wastes: A review of contemporary treatment, recycling and management strategies", Sustainable Chemistry and Pharmacy, 30, 100865, 2022. https://doi.org/10.1016/j.jscsp.2022.100865

[3] Zhao, L., Deng, J., Sun, P., Liu, J., Ji, Y., Nakada, N., Qiao, Z., Tanaka, H., Yang, Y. "Nanomaterials for treating emerging contaminants in water by adsorption and photocatalysis: Systematic review and bibliometric analysis", Science of The Total Environment, 627, pp. 1253–1263, 2018. https://doi.org/10.1016/j.scitotenv.2018.02.006

[4] Stacciarini, J. H. S. "The consolidation of the pharmaceutical sector in the global economy: Growth, influence, deviations, and marketing", PhD Thesis, Federal University of Goiás (UFG), Brazil, 2023.

[5] Scheurer, M., Michel, A., Brauch, H. J., Ruck, W., Sacher, F. "Occurrence and fate of the antidiabetic drug metformin and its metabolite guanylurea in the environment and during drinking water treatment", Water Research, 46(15), pp. 4790–4802, 2012. https://doi.org/10.1016/j.watres.2012.06.019

[6] Haiba, E., Nei, L., Herodes, K., Ivask, M., Lillenberg, M. "On the degradation of metformin and carbamazepine residues in sewage sludge compost", Agronomy Research, 16(3), pp. 696–707, 2018. https://doi.org/10.15159/AR.18.123

[7] Bechambi, O., Sayadi, S., Najjar, W. "Photocatalytic degradation of bisphenol A in the presence of C-doped ZnO: Effect of operational parameters and photodegradation mechanis", Journal of Industrial and Engineering Chemistry, 32, pp. 201–210, 2015. https://doi.org/10.1016/j.jiec.2015.08.017

[8] Snehamol, M., Ganguly, P., Kumaravel, V., Harrison, J., Hinder, S. J., Bartlett, J., Pillai, S. C. "Effect of chalcogens (S, Se, and Te) on the anatase phase stability and photocatalytic antimicrobial activity of TiO_2", Materials Today: Proceedings, 33, pp. 2458–2464, 2020. https://doi.org/10.1016/j.matpr.2020.01.336

[9] Kosmulski, M. "The pH-dependent surface charging and points of zero charge", Journal of Colloid and Interface Science, 253(1), pp. 77–87 2002. https://doi.org/10.1006/jcis.2002.8490

[10] Daneshvar, N., Salari, D., Khataee, A. R. "Photocatalytic degradation of azo dye acid red 14 in water: Investigation of the effect of operational parameters", Journal of Photochemistry and Photobiology A: Chemistry, 157(1), pp. 111–116 2003. https://doi.org/10.1016/S1010-6030(03)00015-7

[11] International Centre for Diffraction Data "Powder Diffraction File (PDF-2), Card No. 36-1451 (ZnO, hexagonal wurtzite structure)", ICDD, Newtown Square, PA, USA, 2006.

[12] Tao, Y., Cheng, Z., Ting, K. E., Yin, X. J. "Studies of photocatalytic kinetics on the degradation of bisphenol A (BPA) by immobilized ZnO nanoparticles in aerated photoreactors", Journal of Environmental Science and Engineering A, 1, pp. 187–194, 2012.

[13] De la Cruz, N., Esquius, L, Grandjean, D., Magnet, A., Tungler, A., de Alencastro, L.F., Pulgarín, C. "Degradation of emergent contaminants by UV, UV/H_2O_2 and neutral photo-Fenton at pilot scale in a domestic wastewater treatment plant", Water Research, 47(15), pp. 5836–5845, 2013. https://doi.org/10.1016/j.watres.2013.07.005

[14] Herrmann, J. M. "Heterogeneous photocatalysis: Fundamentals and applications to the removal of various types of aqueous pollutants", Catalysis Today, 53(1), pp. 115–129, 1999. https://doi.org/10.1016/S0920-5861(99)00107-8

[15] Jasso-Salcedo, A., Meimaroglou, D., Camargo, M., Hoppe, S., Pla, F., Escobar-Barrios, V. "A new catalytic system for the photodegradation of endocrinal disruptors: Synthesis and efficiency modeling and optimization", Chemical Engineering Transactions, 43, pp. 937–942, 2015. https://doi.org/10.3303/CET1543157

[16] Zacharakis, A., Chatzisymeon, E., Binas, V., Frontistis, Z., Venieri, D., Mantzavinos, D. "Solar photocatalytic degradation of bisphenol A on immobilized ZnO or TiO_2", International Journal of Photoenergy, 2013(1), 570587, 2013. https://doi.org/10.1155/2013/570587

[17] Xekoukoulotakis, N. P., Drosou, C., Brebou, C., Chatzisymeon, E., Hapeshi, E., Fatta-Kassinos, D., Mantzavinos, D. "Kinetics of UV-A/TiO_2 photocatalytic degradation and mineralization of the antibiotic sulfamethoxazole in aqueous matrices", Catalysis Today, 161(1), pp. 163–168, 2011. https://doi.org/10.1016/j.cattod.2010.09.027

[18] Galindo, C., Jacques, P., Kalt, A. "Photooxidation of the phenylazonaphthol AO20 on TiO_2: Kinetic and mechanistic investigations", Chemosphere, 45(6–7), pp. 997–1005, 2001. https://doi.org/10.1016/S0045-6535(01)00118-7

[19] Chong, M. N., Jin, B., Chow, C. W. K., Saint, C. "Recent developments in photocatalytic water treatment technology: A review", Water Research, 44(10), pp. 2997–3027, 2010. https://doi.org/10.1016/j.watres.2010.02.039

[20] Gad-Allah, T. A., Ali, M. E. M., Badawy, M. I. "Photocatalytic oxidation of ciprofloxacin under simulated sunlight", Journal of Hazardous Materials, 186(1), pp. 751–755, 2011. https://doi.org/10.1016/j.jhazmat.2010.11.066

[21] Abellán, M. N., Bayarri, B., Giménez, J., Costa, J. "Photocatalytic degradation of sulfamethoxazole in aqueous suspension of TiO_2", Applied Catalysis B: Environmental, 74(3–4), pp. 233–241, 2007. https://doi.org/10.1016/j.apcatb.2007.02.017

[22] Ahmed, S., Rasul, M. G., Martens, W. N., Brown, R., Hashib, M. A. "Heterogeneous photocatalytic degradation of phenols in wastewater: A review on current status and developments", Desalination, 261(1–2), pp. 3–18, 2010. https://doi.org/10.1016/j.desal.2010.04.062

[23] Hoffmann, M. R., Martin, S. T., Choi, W., Bahnemann, D. W. "Environmental applications of semiconductor photocatalysis", Chemical Reviews, 95(1), pp. 69–96, 1995. https://doi.org/10.1021/cr00033a004

[24] Elmolla, E. S., Chaudhuri, M. "Degradation of amoxicillin, ampicillin and cloxacillin antibiotics in aqueous solution by the UV/ZnO photocatalytic process", Journal of Hazardous Materials, 173(1–2), pp. 445–449, 2010. https://doi.org/10.1016/j.jhazmat.2009.08.104

[25] Yadav, A. K., Kumar, A., Singh, S., Kumar, S. "Photocatalytic degradation of pharmaceutical pollutants using ZnO-based nanomaterials: A review", Environmental Technology & Innovation, 24, 101821, 2021. https://doi.org/10.1016/j.eti.2021.101821

[26] Gaya, U. I., Abdullah, A. H. "Heterogeneous photocatalytic degradation of organic contaminants over titanium dioxide: A review of fundamentals, progress, and problems", Journal of Photochemistry and Photobiology C: Photochemistry Reviews, 9(1), pp. 1–12, 2008. https://doi.org/10.1016/j.jphotochemrev.2007.12.003

[27] Kumar, R., Akbarinejad, A., Jasemizad, T., Fucina, R., Travas-Sejdic, J., Padhye, L. P. "The removal of metformin and other selected PPCPs from water by poly(3,4-ethylenedioxythiophene) photocatalyst", Science of the Total Environment, 751, 142302, 2021. https://doi.org/10.1016/j.scitotenv.2020.142302

[28] Ollis, D. F., Pelizzetti, E., Serpone, N. "Photocatalyzed destruction of water contaminants", Environmental Science & Technology, 25(9), pp. 1522–1529, 1991. https://doi.org/10.1021/es00021a001

[29] Hou, D., Goei, R., Wang, X., Wang, P., Lim, T. T. "Preparation of carbon-sensitized and Fe-Er codoped TiO_2 with response surface methodology for bisphenol A photocatalytic degradation under visible-light irradiation", Applied Catalysis B: Environmental, 126, pp. 121–133, 2012. https://doi.org/10.1016/j.apcatb.2012.07.012

[30] Šimůnek, J., van Genuchten, M. T., Šejna, M. "Development and applications of the HYDRUS and STANMOD software packages and related codes", Vadose Zone Journal, 7(2), pp. 587–600, 2008. https://doi.org/10.2136/vzj2007.0077

[31] Boithias, L., Sauvage, S., Srinivasan, R., Leccia, O., Sánchez-Pérez, J. M. "Coupling pesticide fate and transport models in soil: A review", Environmental Modelling & Software, 55, pp. 1–15, 2014. https://doi.org/10.1016/j.envsoft.2014.01.004

[32] Bouredji, H., Bendjaballah Lalaoui, N., Rennane, S., Merzougui, A. "Predicting solute transport parameters in saturated porous media using hybrid algorithm", Iranian Journal of Chemistry & Chemical Engineering, 40(3), pp. 945–954, 2020. https://doi.org/10.30492/ijcce.2020.38103

[33] Foo, K. Y., Hameed, B. H. "Insights into the modeling of adsorption isotherm systems", Chemical Engineering Journal, 156(1), pp. 2–10, 2010. https://doi.org/10.1016/j.cej.2009.09.013

[34] Weber, W. J., Morris, J. C. "Kinetics of adsorption on carbon from solution", Journal of the Sanitary Engineering Division, 89(2), pp. 31–60, 1963. https://doi.org/10.1061/JSEDAI.0000430

[35] Freundlich, H. "Über die Adsorption in Lösungen" (About Adsorption in Solutions), Zeitschrift für Physikalische Chemie, 57(1), pp. 385–470, 1907. (in German) https://doi.org/10.1515/zpch-1907-5723

[36] Leij, F. J., Bradford, S. A. "Combined physical and chemical nonequilibrium transport model: Analytical solution, moments, and application to colloids", Journal of Contaminant Hydrology, 110(3–4), pp. 87–99, 2009. https://doi.org/10.1016/j.jconhyd.2009.09.004

[37] Bouredji, H., Bendjaballah-Lalaoui, N., Merzougui, A., Rennane, S. "Modeling solute transport in saturated soil column: Coupling physical non-equilibrium model and nonlinear Freundlich isotherm", Journal of Porous Media", 24(4), pp. 19–35, 2021. https://doi.org/10.1615/JPorMedia.2021033301

[38] Briones, R. M., Sarmah, A. K. "Sorption and mobility of metformin and guanylurea in soils as affected by biosolid amendment: Batch and column tests", Environmental Pollution, 244, pp. 19–27, 2019. https://doi.org/10.1016/j.envpol.2018.10.025